Zinc Gallogermanate Solid Solution: A Novel Photocatalyst for Efficiently Converting CO_2 into Solar Fuels

Shicheng Yan, Jiajia Wang, Honglin Gao, Nanyan Wang, He Yu, Zhaosheng Li, Yong Zhou,* and Zhigang Zou**

As global energy demand continues to grow, the need to find a carbon-neutral and sustainable energy source for future generations has become imperative. An especially attractive solution is to store solar energy in the form of chemical fuel via artificial photosynthesis to convert carbon dioxide into hydrocarbons. An artificial photosynthesis system is introduced based on a zinc gallogermanate solid solution photocatalyst that can convert the carbon dioxide and water into methane. The solid solution of cubic spinel $ZnGa_2O_4$ and pseudocubic inverse spinel Zn_2GeO_4 is successfully synthesized by hydrothermal ion exchange reaction. Introducing Zn_2GeO_4 into $ZnGa_2O_4$ can effectively narrow band gap by the upshift of valence band edge from the enhanced p-d (O2p-Zn3d) repulsion effect by incorporating s and p orbitals of Ge, and the downshift of conduction band edge by introducing the low-energy s orbital of Ge. The zinc gallogermanate solid solution has a light-hole effective mass, which is beneficial to improving hole mobility, and thus enhancing the ability of photocatalyst in water oxidation to provide protons for CO_2 photoreduction. As a result of band gap narrowing and high hole mobility, the zinc gallogermanate solid solution exhibits high activity in converting CO_2 and H_2O into CH_4 and O_2.

1. Introduction

There is increasing interest in the use of solar energy to drive the photoreduction of carbon dioxide into valuable organic materials using a semiconductor-particle photocatalyst. For solar fuel production by photocatalysis, despite decades of research, the quest for a photocatalyst with all of the characteristics required for artificial photosynthesis has proved unsuccessful, and the reported solar-to-chemical energy conversion efficiencies are still too low to make these systems commercially viable.[1] One strategy that can be used to enhance the photocatalytic activity of a given semiconductor photocatalyst is to construct a solid-solution photocatalyst. A series of solid-solution photocatalysts, such as $AgGa_{1-x}Al_xO_2$,[2a] $(AgIn)_xZn_{2(1-x)}S_2$,[2b] $Zn_{1-x}Cu_xS$,[2c] ZnS-$CuInS_2$-$AgInS_2$,[2d] $(SrTiO_3)_{1-x}(LaTiO_2N)_x$,[2e] $In_xGa_{1-x}N$,[2f] and GaN:ZnO,[2g] have been developed. The solid solutions exhibit better performance than the single components comprising the solid solution, which has been demonstrated in photocatalytic water splitting and pollutant degradation.

Photocatalysts with d^{10} electronic configuration, such as $ZnGa_2O_4$ and Zn_2GeO_4, exhibit high photocatalytic activity in water splitting due to the large energy dispersion of the bottom of the conduction band which is able to yield excited electrons with large mobility useful for photocatalysis.[3] Here, our aim is to synthesize a novel solid solution of cubic spinel $ZnGa_2O_4$ and pseudocubic inverse spinel Zn_2GeO_4 to drive the photoreduction of CO_2 into hydrocarbon fuels. The zinc gallogermanate solid solution can be synthesized by a hydrothermal ion-exchange reaction, and it exhibits improved photocatalytic performance in converting CO_2 to CH_4 due to the band gap narrowing from an enhanced p-d repulsion effect in the valence band, the introduction of a low-energy s orbital of Ge in the conduction band, and the high hole mobility due to the light effective mass of the holes.

Prof. S. C. Yan, Dr. J. J. Wang, Dr. H. L. Gao, Prof. Z. S. Li
Department of Materials Science and Engineering
College of Engineering and Applied Sciences
NO. 22, Hankou Road, Nanjing, Jiangsu 210093, China
E-mail: yscfei@nju.edu.cn
N. Y. Wang, H. Yu, Prof. Y. Zhou, Prof. Z. G. Zou
Eco-Materials and Renewable Energy Research Center (ERERC)
National Laboratory of Solid State Microstructures
Nanjing University
NO. 22, Hankou Road, Nanjing, Jiangsu 210093, China
E-mail: zhouyong1999@nju.edu.cn; zgzou@nju.edu.cn

DOI: 10.1002/adfm.201202484

2. Results and Discussion

2.1. Hydrothermal Ion Exchange Route to Prepare Zinc Gallogermanate Solid Solution

The zinc gallogermanate was synthesized by hydrothermal ion-exchange reaction, as described in the Experimental Section. In brief, the precursor, $K_{0.9}Ga_{0.9}Ge_{0.1}O_2$, was first prepared by solid state reaction (see Figure S1 in the Supporting Information) and dispersed in water to form a colloidal suspension (see Figure S2 in the Supporting Information). After Zn^{2+}

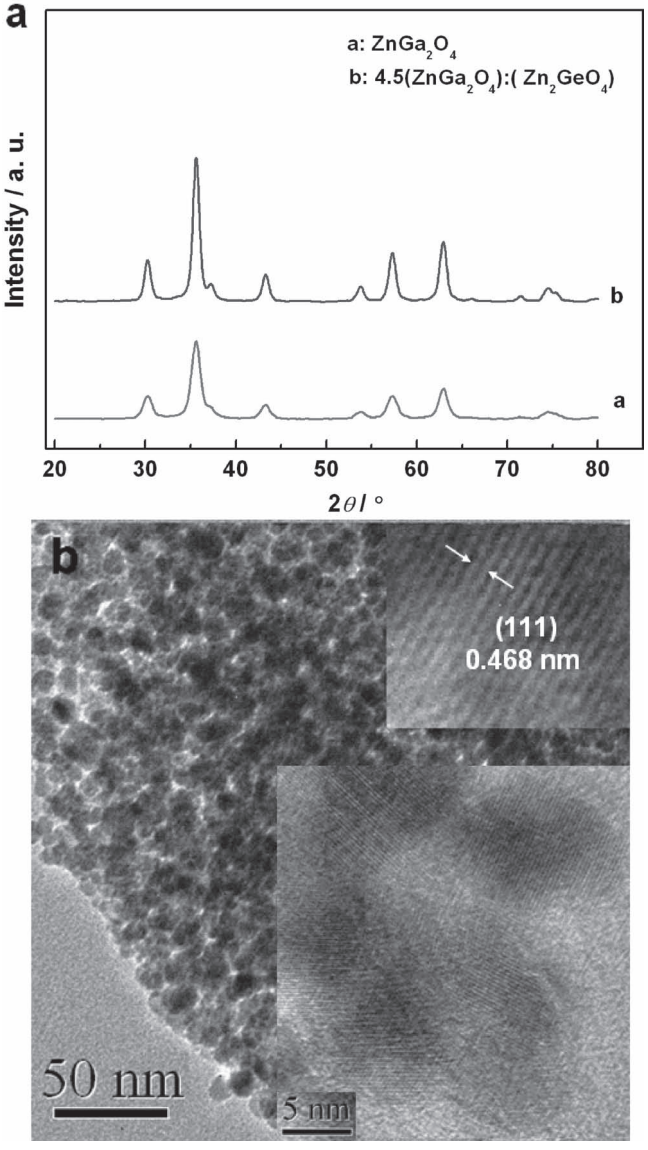

Figure 1. XRD and TEM results. a) XRD patterns for the zinc gallogermanate solid solution and $ZnGa_2O_4$. b) TEM image for the zinc gallogermanate solid solution. Insets show the high-resolution lattice images.

from $Zn(CH_3COO)_2$ aqueous solution was introduced into the $K_{0.9}Ga_{0.9}Ge_{0.1}O_2$ colloidal suspension, hydrothermal treatment was carried out to obtain the zinc gallogermanate (denoted as 4.5($ZnGa_2O_4$):(Zn_2GeO_4)). For comparison, $ZnGa_2O_4$ was prepared by hydrothermal ion-exchange reaction between $NaGaO_2$ and $Zn(CH_3COO)_2$, as described in our previous report.[4]

The XRD pattern of zinc gallogermanate (**Figure 1**a) is very similar to that of $ZnGa_2O_4$, and the two as-prepared samples can be indexed as cubic phase $ZnGa_2O_4$ (JCPDS 38-1240), indicating that the cubic zinc gallogermanate formed via the ion exchange reaction of $10K_{0.9}Ga_{0.9}Ge_{0.1}O_2+6.5Zn(CH_3COO)_2+2H_2O \rightarrow 4.5(ZnGa_2O_4):(Zn_2GeO_4)+9CH_3COOK+4CH_3COOH$. Compared with the $ZnGa_2O_4$, all XRD peaks of zinc gallogermanate shift toward higher 2θ values because the ion radius of Ge^{4+} (0.053 nm) is smaller than that of Ga^{3+} (0.062 nm). The calculated lattice parameter based on XRD data is a = 8.339 Å for zinc gallogermanate, which is smaller than the cubic $ZnGa_2O_4$ (a = 8.366 Å) and larger than the pseudocubic Zn_2GeO_4 (a = 8.300 Å).[5] The TEM observation (Figure 1b) indicates that the as-prepared zinc gallogermanate exhibits a wormhole framework. The high-resolution TEM (HRTEM) image shows that the mesostructure resulted from aggregation of the nanocrystals with a particle size of about 10 nm (inset in Figure 1b). The HRTEM analysis also indicates that the lattice spacing is 0.468 nm for the (111) plane of the zinc gallogermanate, which is smaller than 0.481 nm for the (111) plane of $ZnGa_2O_4$, further confirming that the Ge atom was introducing into the $ZnGa_2O_4$. These evidences may support the standpoint that the as-prepared zinc gallogermanate is a solid solution composed of cubic $ZnGa_2O_4$ and pseudocubic Zn_2GeO_4.

For $ZnGa_2O_4$, the cubic spinel $ZnGa_2O_4$ is an easily obtainable and stable compound.[4] However, Zn_2GeO_4 has a phenacite structure (rhombohedral phase) at atmospheric pressure.[6] At 1100 °C, under 3.5 GPa, the rhombohedral phenacite-type Zn_2GeO_4 transformed completely to a slightly distorted spinel structure (pseudocubic phase), meaning that the pseudocubic Zn_2GeO_4 is a high-temperature and high-pressure phase.[5] To further confirm the composition of the as-prepared zinc gallogermanate, X-ray photoelectron spectroscopy (XPS) and energy dispersive spectroscopy (EDS) analysis was carried out. For the as-prepared zinc gallogermanate, the atomic ratios for Zn/Ga, Zn/Ge, Ga/Ge and Zn/O confirmed by XPS and EDS are very close to the theoretical values (see Table S1 in the Supporting Information), that is, the mole ratio of $ZnGa_2O_4$ to Zn_2GeO_4 is 4.5:1. The strong Ge $2p_{3/2}$ signal in the XPS spectra of the as-prepared zinc gallogermanate was detected to be at 1219.31 eV (**Figure 2**a), which is smaller than 1219.8 eV for rhombohedral Zn_2GeO_4 and 1220.2 eV for GeO_2,[7] meaning that a novel bond formed. A slight decrease in Ga 2p and O 1s binding energies as well as a slight increase in Zn 2p binding energies for the zinc gallogermanate (Ga $2p_{3/2}$ at 1117.19 eV, O 1s at 530.12 eV and Zn $2p_{3/2}$ at 1020.95 eV) than $ZnGa_2O_4$ (Ga $2p_{3/2}$ at 1117.37 eV, O1s at 530.45 eV and Zn $2p_{3/2}$ at 1021.28 eV) was observed (Figure 2b–d). The change in binding energies would result from that the Ge element was introduced into the $ZnGa_2O_4$. The energetic separation (ΔE) between the Zn $2p_{3/2}$ and Ga $2p_{3/2}$ peaks can be used as a sensitive tool to confirm the formation of spinel $ZnGa_2O_4$. A small ΔE value means that more complete phase transformation to cubic spinel structure occurs. Here, the ΔE value was determined to be 96.11 eV for $ZnGa_2O_4$ and 96.21 eV for zinc gallogermanate, which is much lower than 96.7 eV for the mixture of ZnO and Ga_2O_3,[8] indicating that cubic spinel structure formed, as demonstrated by XRD. A slight increase in ΔE value for zinc gallogermanate compared with $ZnGa_2O_4$ further confirmed that zinc gallogermanate is a solid solution of the pseudocubic Zn_2GeO_4 and cubic $ZnGa_2O_4$.

Based on the XRD and XPS analysis, we can conclude that the high-temperature and high-pressure compound, pseudocubic spinel Zn_2GeO_4, can be easily formed by using the gallogermanate as the reaction precursor. The formation of pseudocubic spinel Zn_2GeO_4 is not from the phenacite-spinel high-pressure transformation process which was demonstrated in previous report.[5] The high pressure transformation in Zn_2GeO_4 is an

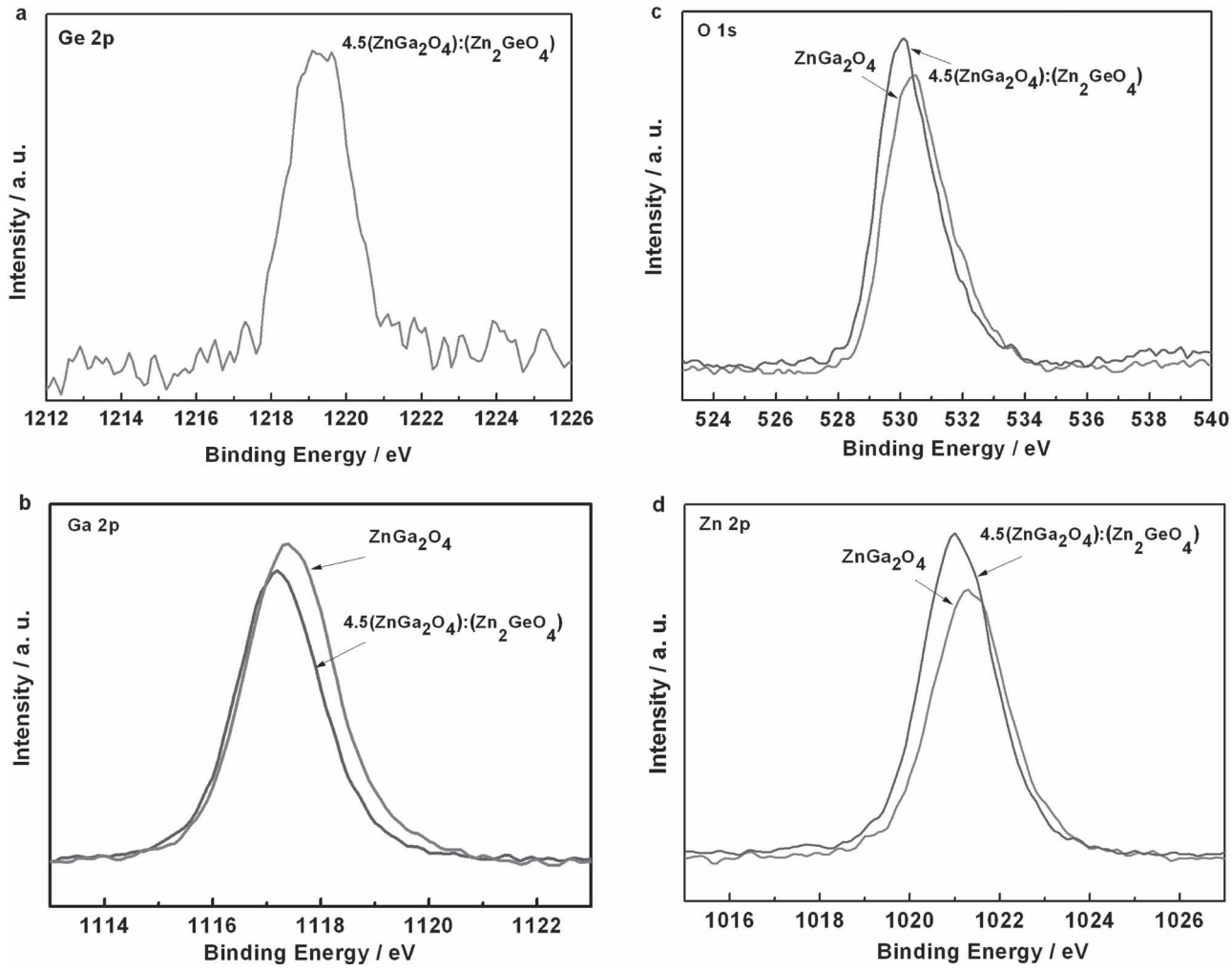

Figure 2. XPS spectra of the as-prepared zinc gallogermanate solid solution and $ZnGa_2O_4$: a) Ge 2p, b) Ga 2p, c) O 1s, and d) Zn 2p.

important phase transformation process, which has important applications to studies of the constitution of the Earth's mantle. Here, we found a mild route to pseudocubic spinel Zn_2GeO_4 by hydrothermal ion-exchange reaction between potassium gallogermanate and Zn^{2+}. This means that the pseudocubic spinel Zn_2GeO_4 can be formed under a mild geologic condition by forming gallogermanate associated minerals.

Nitrogen adsorption-desorption studies indicated that both the as-prepared $4.5(ZnGa_2O_4):(Zn_2GeO_4)$ and $ZnGa_2O_4$ (see Figure S3 in the Supporting Information) showed a type IV isotherm, typical of mesoporous materials. The calculated results based on nitrogen adsorption-desorption data indicated that the $4.5(ZnGa_2O_4):(Zn_2GeO_4)$ (5.1 nm, 85.2 $m^2\ g^{-1}$) exhibited a similar pore diameter and specific surface area to the $ZnGa_2O_4$(6.1 nm, 95.3 $m^2\ g^{-1}$). It was well demonstrated in our previous report that the formation of mesopores in $ZnGa_2O_4$ can be caused by the ion-exchange process between Zn^{2+} and Na^+ taking place based on the $NaGaO_2$ mesoporous framework, and then $ZnGa_2O_4$ crystal particles can nucleate and grow there.[4] In present case, $K_{0.9}Ga_{0.9}Ge_{0.1}O_2$ can be dispersed in water, similar to $NaGaO_2$, to form the colloidal suspension with a low zeta potential of –24.5 mV (pH = 8) (see Figure S2 in the Supporting Information). A low zeta potential means that the colloidal particles can aggregate easily to form a mesoporous colloidal framework, as observed by TEM (see Figure S4a in the Supporting Information). The hydrothermal ion-exchange reaction between $K_{0.9}Ga_{0.9}Ge_{0.1}O_2$ and $Zn(CH_3COO)_2$ occurs based on the mesoporous framework to form mesoporous zinc gallogermanate solid solution (see Figure S4b in the Supporting Information).

2.2. Optical Properties and Electronic Band Structure of Zinc Gallogermanate Solid Solution

According to the UV-vis diffuse reflectance spectra (**Figure 3**a), the band gaps for $ZnGa_2O_4$ and $4.5(ZnGa_2O_4):(Zn_2GeO_4)$ were estimated to be 4.45 and 4.18 eV, respectively. Apparently, compared to $ZnGa_2O_4$, the band gap of zinc gallogermanate solid solution narrowed. Valence band XPS (VB XPS) was used for the observation of the valence band electronic state of these as-prepared samples. The valence band edges of $ZnGa_2O_4$

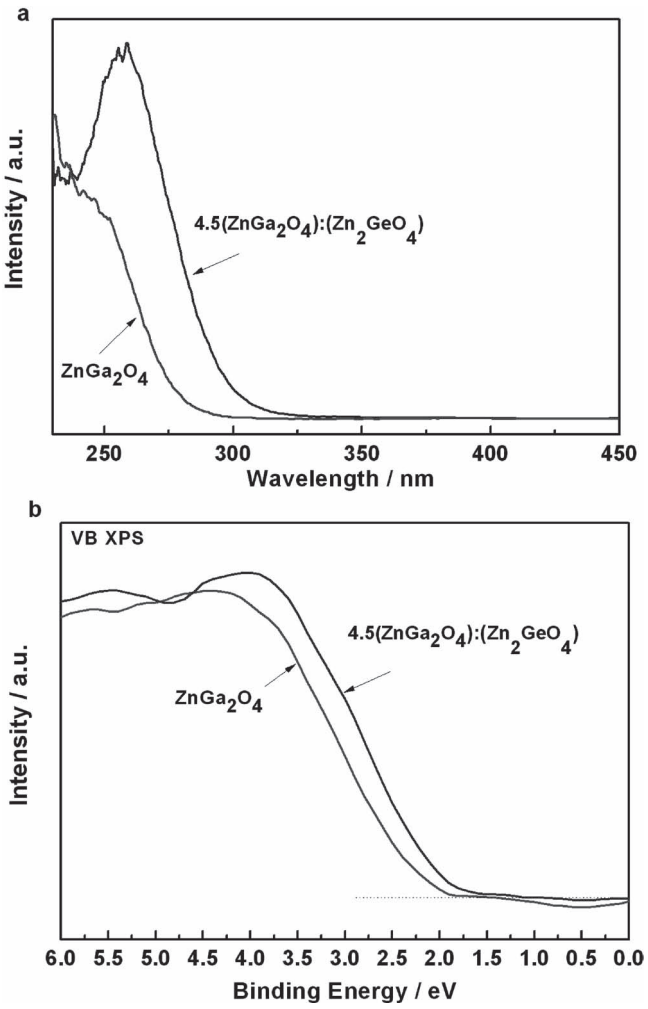

Figure 3. Optical properties and valence band information of the zinc gallogermanate solid solution and $ZnGa_2O_4$. a) UV-vis absorption spectra, and b) VB XPS spectra.

and $4.5(ZnGa_2O_4):(Zn_2GeO_4)$ were estimated to be at +1.95 and +1.82 eV below Fermi level by the linear extrapolation method, respectively (Figure 3b). The conduction band edges of $ZnGa_2O_4$ and $4.5(ZnGa_2O_4):(Zn_2GeO_4)$ located at –2.5 and –2.36 eV, respectively, obtained by $E_g = E_{VB}–E_{CB}$ (E_g: semiconductor band gap; E_{VB}: the valence band edge potential; E_{CB}: the conduction band edge potential). This means that the band gap narrowing by introducing Zn_2GeO_4 into $ZnGa_2O_4$ resulted from the upshift of valence band edge as well as downshift of conduction band edge. The band gap narrowing may promote the photoinduced reaction due to more light absorption.

To understand the electronic structures of the cubic $ZnGa_2O_4$, the pseudocubic Zn_2GeO_4 and their solid solution, density functional theory (DFT) calculations were carried out. We constructed an interface model which consisted of a Zn_2GeO_4 (001) surface and a $ZnGa_2O_4$ (001) surface by sharing two Zn atoms in the interface (**Figure 4**a). Our calculated results indicated that for $ZnGa_2O_4$, the valence band edge is primarily derived from Zn3d and O2p orbitals and the conduction band edge from Ga4s and Zn4s orbitals (see Figure S5a in the Supporting Information). For Zn_2GeO_4 the valence band consisted of hybridized Zn3d and O2p orbitals and the bottom of the conduction band was composed of the Ge4s and Zn4s orbitals (see Figure S5b in the Supporting Information).

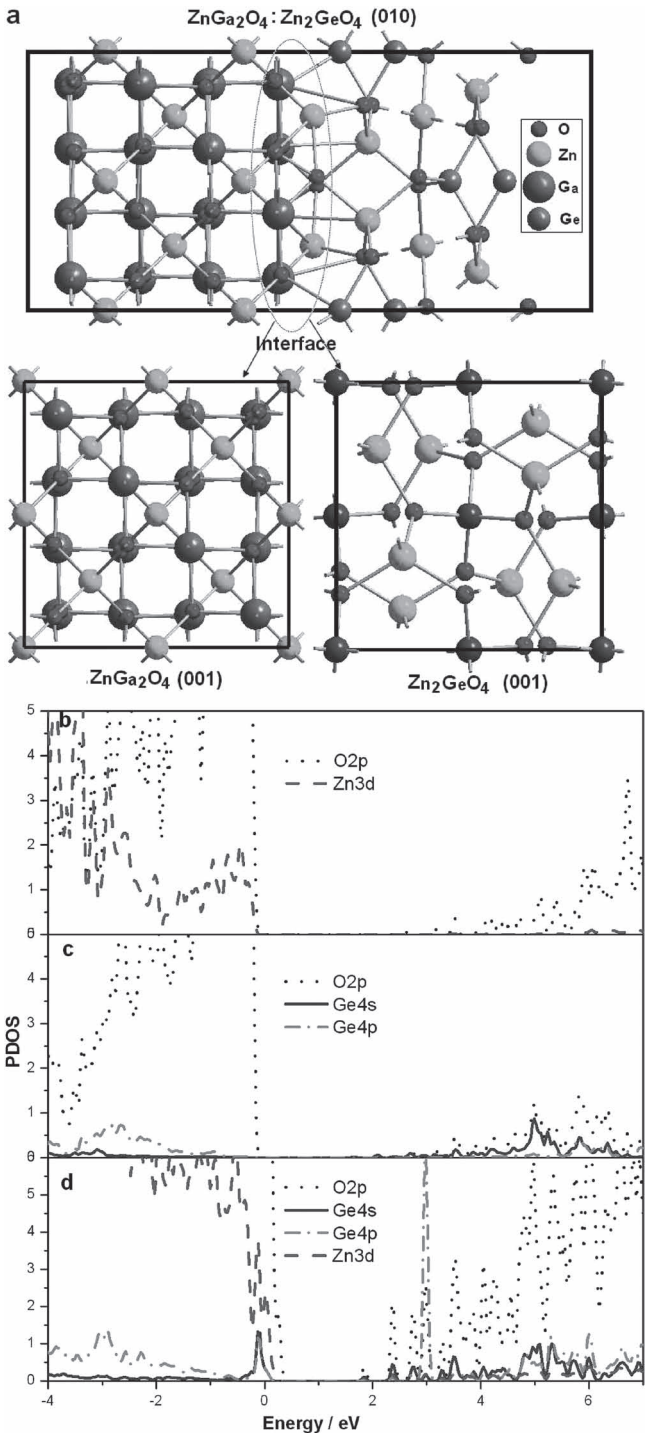

Figure 4. Energy band structures of zinc gallogermanate solid solution, $ZnGa_2O_4$, and pseudocubic cubic Zn_2GeO_4. a) Constructed model of zinc gallogermanate solid solution by connecting both (001) surfaces of $ZnGa_2O_4$ and Zn_2GeO_4. b) PDOS of $ZnGa_2O_4$. c) PDOS of Zn_2GeO_4. d) PDOS of zinc gallogermanate solid solution.

After forming the zinc gallogermanate solid solution, a prominent change is the upshift of the valence band edge as well as the downshift of the conduction band edge, thus narrowing the width of the band gap (see Figure S5c in the Supporting Information), which is in good agreement with the observed results by VB XPS and UV-vis absorption spectra. For a more clear comparison, the calculated projected density of states (PDOS) for $ZnGa_2O_4$, $ZnGe_2O_4$ and zinc gallogermanate solid solution are selectively given in Figure 4b–d, respectively. As can be seen, when Zn_2GeO_4 was incorporated into $ZnGa_2O_4$, interaction between Ge4s4p and O2p results in a bonding and an antibonding orbital in the valence band and the conduction band, respectively, which agrees with the bonding rules in the main group elements.[9] For type II-VI semiconductors, it has been pointed out that p-d repulsion shifts the valence band maximum upwards.[10] Our calculations have shown for a solid solution of $ZnGa_2O_4$ and Zn_2GeO_4, the presence of O2p and Zn3d electrons in the upper valence band provides p-d repulsion for the valence band maximum (Figure 4d). The bonding interactions between Ge4s4p and O2p in the valence band clearly enhanced the p-d repulsion between O2p and Zn3d, thus further shifting upward the valence band edge. The red-shift of the conduction band edge in the solid solution of $ZnGa_2O_4$ and Zn_2GeO_4 originated from the introduction of the Ge4s orbital, because the Ge4s states are deeper in energy than Ga4s and Zn4s states, which has made a significant contribution to band gap narrowing. A similar band gap narrowing phenomena has been found for $ZnGeAs_2$.[11]

2.3. Photocatalytic Performance of Zinc Gallogermanate Solid Solution in CO_2 Reduction

Converting CO_2 into valuable hydrocarbons by means of solar energy is one of the best solutions to both global warming and energy shortage. Here, we use the as-prepared solid solution as a photocatalyst to convert CO_2 into CH_4 under irradiation of UV light. For the photoreduction of CO_2 into solar fuel, a popular reaction is to use H_2O as the reducing agent. **Figure 5** shows that the mesoporous $4.5(ZnGa_2O_4):(Zn_2GeO_4)$ solid solution exhibited a CH_4 yield of about 0.5 μmol during the first hour under light illumination, which is about 33 times higher than mesoporous $ZnGa_2O_4$ (0.015 μmol h^{-1}). Also, a significant rate difference in the O_2 generation was observed during the CO_2 photoreduction. The O_2 generation rate over the $4.5(ZnGa_2O_4):(Zn_2GeO_4)$ solid solution is 2.3 μmol h^{-1}, which is much higher than $ZnGa_2O_4$ (0.47 μmol h^{-1}). A mesoporous structure is usually beneficial for promoting the gas-phase reaction due to the strong gas adsorption by mesopores.[4] In our case of the zinc gallogermanate solid solution and $ZnGa_2O_4$, both the as-prepared samples have a very similar mesoporous structure. The amount of CO_2 adsorbed on the powder samples was evaluated by the BET method at 0 °C to be 6.03 mg g^{-1} for $4.5(ZnGa_2O_4):(Zn_2GeO_4)$, which is very close to 5.96 mg g^{-1}, as measured for $ZnGa_2O_4$. The amount of water adsorbed on the two powder samples was determined gravimetrically under 75% relative humidity at 35 °C to be 0.048 g g^{-1} for $4.5(ZnGa_2O_4):(Zn_2GeO_4)$, which is about 15% lower than 0.057 g g^{-1}, as measured for $ZnGa_2O_4$. This indicates that for the two as-prepared samples, the large activity difference in photoreduction of CO_2 cannot be attributed to the gas adsorption.

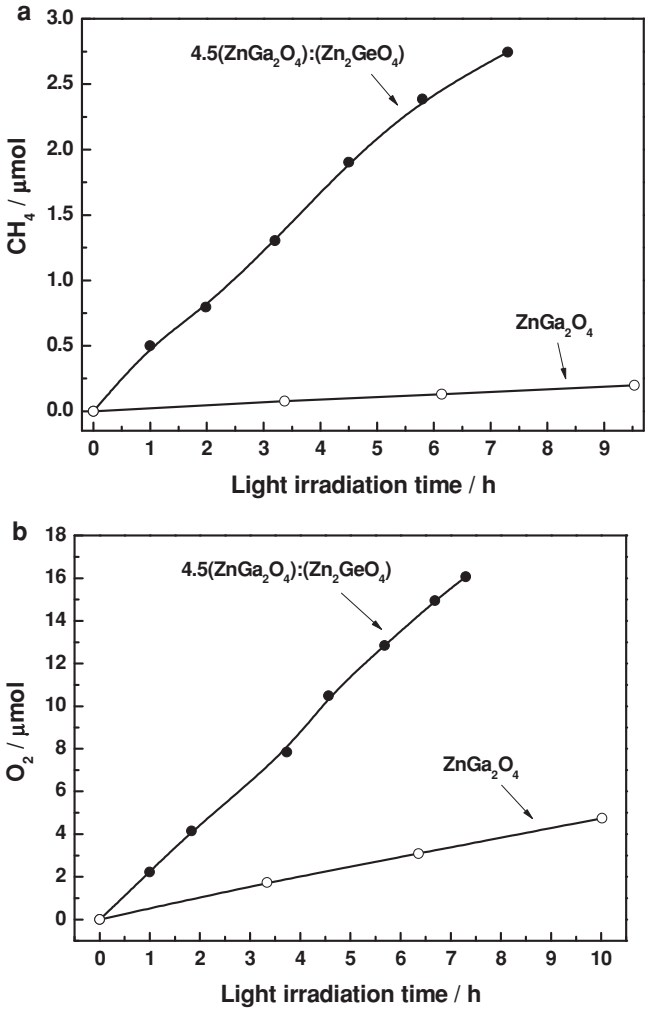

Figure 5. Gaseous product generation over the zinc gallogermanate solid solution and $ZnGa_2O_4$ as a function of irradiation time: a) CH_4; b) O_2.

The CO_2+H_2O photoreduction involves two half-reactions: the photogenerated holes on the valence band top of photocatalyst induce the water oxidation of $2H_2O \rightarrow O_2 + 4H^+ + 4e^-_{CB}$ and the photogenerated electrons on the bottom of the conduction band of the photocatalyst drive the reduction of CO_2 into hydrocarbon fuels such as CH_4 by the reaction of CO_2+ $8e^-$ + $8H^+ \rightarrow CH_4$+ $2H_2O$. We know that during the photoreduction of CO_2, H_2O is oxidized into O_2 and this process provides the protons and electrons, which are the reducing agents that induce the reduction of CO_2 into hydrocarbons. This means that both CO_2 photoreduction as well as water oxidation have to occur simultaneously in a photoreactor. However, oxygen evolution is the major rate-limiting step in water oxidation by photocatalysts, as demonstrated in TiO_2,[12a–d] Fe_2O_3,[12a] and WO_3,[12e] due to slow kinetics of the hole reaction with water. To achieve an efficient photoreduction of CO_2, a photocatalyst with strong water oxidation ability is required. The high O_2 generation rate over the $4.5(ZnGa_2O_4):(Zn_2GeO_4)$ solid solution implied that

the zinc gallogermanate solid solution possesses a strong water oxidation ability compared to $ZnGa_2O_4$. Here, both the zinc gallogermanate and $ZnGa_2O_4$ are nanocrystals with a particle size of about 10 nm (Figure 1b), which allows one to discuss the hole mobility in such materials. For a semiconductor photocatalyst, a light-hole effective mass is desirable for high mobility, which is beneficial for improving the photoactivity. The DFT calculated effective mass of hole for zinc gallogermanate solid solution is 2.13 m_0 (where m_0 is the free electron mass), is much smaller than that of $ZnGa_2O_4$ (3.16 m_0). This indicates that introducing Zn_2GeO_4 into $ZnGa_2O_4$ is able to decrease effective mass of holes, thus improving the kinetics of water oxidation by the photogenerated holes.

The higher photocatalytic activity of the zinc gallogermanate solid solution toward reduction of CO_2 relative to that of the $ZnGa_2O_4$ can be attributed to the following two reasons: (1) The band gap narrowing by introducing Zn_2GeO_4 into $ZnGa_2O_4$ can improve the photocatalytic activity of the photocatalyst due to greater light absorption. (2) Introducing Zn_2GeO_4 into $ZnGa_2O_4$, the water oxidation reaction is enhanced resulting from the high hole mobility, which process can efficiently provide the protons, and thus promoting the CO_2 photoreduction.

3. Conclusions

Using a hydrothermal reaction, we have synthesized a mesoporous solid solution of cubic $ZnGa_2O_4$ and pseudocubic Zn_2GeO_4. Introducing Zn_2GeO_4 into $ZnGa_2O_4$ can effectively narrow the band gap by the upshift of the valence band edge from an enhanced p-d repulsion effect and the downshift of conduction band edge by introduction of the low-energy s orbital of Ge. The zinc gallogermanate solid solution has a light-hole effective mass, which is beneficial to improving the hole mobility, and thus enhancing the ability of the photocatalyst in water oxidation. As a result, the zinc gallogermanate solid solution exhibited high activity in converting CO_2 and H_2O into CH_4 and O_2.

4. Experimental Section

Synthesis and Characterization: $K_{0.9}Ga_{0.9}Ge_{0.1}O_2$ solid powders were synthesized by heating a stoichiometric mixture of Ga_2O_3, GeO_2, and K_2CO_3 at 1000 °C for 12 h. The mesoporous zinc gallogermanate solid solution was prepared by hydrothermal ion exchange. Typically, $K_{0.9}Ga_{0.9}Ge_{0.1}O_2$ colloidal suspension (0.05 M, 20 mL) was added into aquatic solution of $Zn(CH_3COO)_2$ (0.065 M, 10 mL), stirred for 30 min at room temperature, then heated in a Teflon-lined hydrothermal autoclave at 200 °C for 10 h (denoted as $4.5(ZnGa_2O_4):(Zn_2GeO_4)$). For comparison, the mesoporous $ZnGa_2O_4$ was prepared using the same procedure by mixing $NaGaO_2$ colloidal suspension (0.05 M, 20 mL) and aquatic solution of $Zn(CH_3COO)_2$ (0.05 M, 10 mL). These sediments after hydrothermal reaction were separated by centrifugation and dried at 60 °C for 2 h.

The crystalline phases of these as-prepared products were determined by powder XRD (Rigaku Ultima III, CuKa radiation). The specific surface area of the as-prepared samples was measured by nitrogen sorption at 77 K on a surface area and porosity analyzer (Micromeritics TriStar 3000, USA). The pore diameter was calculated from the nitrogen adsorption isotherm by the Barrett–Joyner–Halenda (BJH) method. The specific surface area was calculated from the linear region of the Brunauer–Emmett–Teller (BET) plot ranging from P/P_0 = 0.05 to P/P_0 = 0.15. The morphology of the samples was observed by transmission electron microscope (TEM) (FEI Tecnai G2 F30 S-Twin, USA). X-ray photoelectron spectroscopy (XPS) was undertaken using a Thermo ESCALAB 250 physical electronics photoelectron spectrometer with monochromatized Al-Ka X-ray radiation (1486.6 eV). The energy resolution of the electrons analyzed by the hemispherical mirror analyzer was about 0.2 eV. The binding energy was determined by reference to the C 1s line at 284.8 eV.

Photocatalytic Tests: In the photocatalytic reduction of CO_2, photocatalyst powder (0.1 g) was uniformly dispersed on a glass reactor with an area of 4.2 cm^2. A UV-enhanced (200 to 350 nm) 300W xenon arc lamp was used as the light source for the photocatalytic reaction. The volume of the reaction system was about 230 mL. The reaction setup was vacuum-treated several times, and then high-purity CO_2 gas was introduced into the reaction to achieve ambient pressure. Deionized water (0.4 mL) was injected into the reaction system as the reducing agent. During irradiation, about 1 mL of gas was taken from the reaction cell at given intervals for subsequent CH_4 concentration analysis with a gas chromatograph (GC-2014, Shimadzu Corp., Japan).

Theoretical Calculations: First principle calculations were used to identify the effects of the Zn_2GeO_4 phase on the physical properties of the host $ZnGa_2O_4$. Since the lattice parameter of Zn_2GeO_4 (a = 8.300 Å) is comparable with that of $ZnGa_2O_4$ (a = 8.366 Å), we constructed an interface model which consisted of both Zn_2GeO_4 and $ZnGa_2O_4$. Bulk Zn_2GeO_4 and $ZnGa_2O_4$ were firstly relaxed. Then, the Zn_2GeO_4 (001) surface was connected to the $ZnGa_2O_4$ (001) surface by sharing two Zn atoms in the interface. Therefore, this interface model consisted of 48 O, 14 Zn, 16 Ga, and 4 Ge atoms ($Zn_7Ga_{16}O_{32}$ and $Zn_7Ge_4O_{16}$). 10-Å vacuum regions were added to eliminate interactions between two images. During relaxation, two-atom thick layers of each side in the interface model were fixed at bulk positions.

The density functional theory (DFT) calculations were performed using the VASP code[13a,b] with the projected augmented wave (PAW) method.[13c] Generalized gradient approximation (GGA)[13d] in the scheme of Perdew–Bueke–Ernzerhof (PBE)[13e] was used for the exchange correlation functional. The valence configurations of the pseudopotentials were $2s^22p^4$ for O, $3d^{10}4s^2$ for Zn, $3d^{10}4s^24p^1$ for Ga and $3d^{10}4s^24p^2$ for Ge. The cutoff energy of the basis function was 500 eV. A Monkhorst–Pack k-point set of $3 \times 3 \times 1$ was used for the interface model. Geometry relaxation was performed until the residual forces on each ion converged to be smaller than 0.02 eV/Å.

Supporting Information

Supporting Information is available from the Wiley Online Library or from the author.

Acknowledgements

This work was supported by the National Basic Research Program of China (973 Program, 2013CB632404), the National Natural Science Foundation of China (Nos. 51102132, 11174129, 51272101, and 51272102), the Priority Academic Program Development of Jiangsu Higher Education Institutions, and the Jiangsu Provincial Funds for Distinguished Young Scientists (No. BK2012015).

Received: August 30, 2012
Published online: November 1, 2012

[1] a) W. Y. Teoh, J. A. Scott, R. Amal, *J. Phys. Chem. Lett.* **2012**, *3*, 629; b) X. B. Chen, S. H. Shen, L. J. Guo, S. S. Mao, *Chem. Rev.* **2010**, *110*, 6503; c) F. E. Osterloh, *Chem. Mater.* **2008**, *20*, 35.

[2] a) S. X. Ouyang, J. H. Ye, *J. Am. Chem. Soc.* **2011**, *133*, 7757; b) I. Tsuji, H. Kato, H. Kobayashi, A. Kudo, *J. Am. Chem. Soc.*

2004, *126*, 13406; c) A. Kudo, M. Sekizawa, *Catal. Lett.* **1999**, *58*, 241; d) I. Tsuji, H. Kato, A. Kudo, *Chem. Mater.* **2006**, *18*, 1969; e) W. J. Luo, Z. S. Li, X. J. Jiang, T. Yu, L. F. Liu, X. Y. Chen, J. H. Ye, Z. G. Zou, *Phys. Chem. Chem. Phys.* **2008**, *10*, 6717; f) W. J. Luo, B. Liu, Z. S. Li, Z. L. Xie, D. J. Chen, Z. G. Zou, R. Zhang, *Appl. Phys. Lett.* **2008**, *92*, 262110; g) S. C. Yan, Z. Q. Wang, Z. S. Li, Z. G. Zou, *J. Mater. Chem.* **2011**, *21*, 5682.

[3] Y. Inoue, *Energy Environ. Sci.* **2009**, *2*, 364.

[4] S. C. Yan, S. X. Ouyang, J. Gao, M. Yang, J. Y. Feng, X. X. Fan, L. J. Wan, Z. S. Li, J. H. Ye, Y. Zhou, Z. G. Zou, *Angew. Chem. Int. Ed.* **2010**, *49*, 6400.

[5] A. E. Ringwood, A. Major, *Nature* **1967**, *215*, 1367.

[6] S. C. Yan, L. J. Wan, Z. S. Li, Z. G. Zou, *Chem. Commun.* **2011**, *47*, 5632.

[7] V. B. R. Boppana, N. D. Hould, R. F. Lobo, *J. Solid State Chem.* **2011**, *184*, 1054.

[8] a) A. R. Phani, S. Santucci, S. DiNardo, L. Lozzi, M. Passacantando, P. Picozzi, P. Cantalni, *J. Mater. Sci.* **1998**, *33*, 3969; b) L. Zou, X. Xiang, M. Wei, F. Li, D. G. Evans, *Inorg. Chem.* **2008**, *47*, 1361.

[9] A. J. Bridgeman, G. Cavigliasso, *Polyhedron* **2001**, *20*, 2269.

[10] S. H. Wei, A. Zunger, *Phys. Rev. B* **1988**, *37*, 8958.

[11] A. Janotti, S. H. Wei, S. B. Zhang, S. Kurtz, *Phys. Rev. B* **2001**, *63*, 195210.

[12] a) J. Cowan, C. J. Barnett, S. R. Pendlebury, M. Barroso, K. Sivula, M. Grätzel, J. R. Durrant, D. R. Klug, *J. Am. Chem. Soc.* **2011**, *133*, 10134; b) J. W. Tang, J. R. Durrant, D. R. Klug, *J. Am. Chem. Soc.* **2008**, *130*, 13885; c) A. J. Cowan, J. W. Tang, W. Leng, J. R. Durrant, D. R. Klug, *J. Phys. Chem. C* **2010**, *114*, 4208; d) K. Iwata, T. Takaya, H. Hamaguchi, A. Yamakata, T. Ishibashi, H. Onishi, H. Kuroda, *J. Phys. Chem. B* **2004**, *108*, 20233; e) F. M. Pesci, A. J. Cowan, B. D. Alexander, J. R. Durrant, D. R. Klug, *J. Phys. Chem. Lett.* **2011**, *2*, 1900.

[13] a) G. Kresse, J. Furthmuller, *Comput. Mater. Sci.* **1996**, *6*, 15; b) G. Kresse, J. hafner, *Phys. Rev. B* **1993**, *47*, 558; c) P. E. Blochl, *Phys. Rev. B* **1994**, *50*, 17953; d) J. P. Perdew, J. A. Chevary, S. H. Vosko, K. A. Jackson, M. R. Pederson, D. J. Singh, C. Fiolhais, *Phys. Rev. B* **1992**, *46*, 6671; e) J. P. Perdew, K. Bruke, M. Ernzerhof, *Phys. Rev. Lett.* **1996**, *77*, 3865.